FINAL TECHNICAL REPORT

FOR

NASA GRANT - NAG-1-488

AN ANALYSIS OF DOPING MODULATED SUPERLATTICE STRUCTURES

Period: June 1, 1984 to May 31, 1985

Principal Investigator: A. M. Buoncristiani

NASA Technical Officer: Dr. Charles E. Byvik

Submitted by:

Department of Physics

Christopher Newport College

Newport News, Virginia 23606

May 31, 1985

TABLE OF CONTENTS

I. SYNOPSIS

A new method of growing doping modulated superlattice structures had been proposed by researchers at the NASA, Langley Research Center. This method utilized organo-metallic chemical vapor deposition (MO-CVD) with the added feature of a controlled plasma in the growth regions. It was anticipated that the presence of the plasma would lower the temperature required for crystal growth and thus enhance the quality of the superlattices fabricated in this way. The main objective of the research undertaken with this grant was to study how the growth environment effected the electronic and optical properties of the superlattice structures. Two experimental stations, a Hall probe to measure carrier concentrations and mobilities and a luminenscence spectrometer were prepared; descriptions of these stations appear in this report. Because a serious safety hazard was discovered in the proposed growth process no superlattice structures were fabricated and the research on this material had to be terminated. The nature of this hazard is as follows:

Beryllium was to be the p-type dopant for the superlattices, transported by a carrier gas to the plasma reaction chamber. The unreacted gases, still containing some beryllium, had then to be disposed of. Because of the toxicity of elemental beryllium it could not be exhausted into the atmosphere. No adequate means of disposing of it or of insuring that traces would not remain trapped in the flow volume was found. It was decided that it was unsafe to proceed with this experiment. (Similar decisions seem to have been reached by other laboratories considering similar methods of fabricating semiconducting devices).

Fortunately, an opportunity to utilize the luminescence experiment for the study of the optical properties of dopant ions in insulating laser hosts arose. The remainder of effort in this grant was expended in initiating a

study of materials suitable for tunable solid state lasers. This work was quite successful, and papers describing the results have been delivered at four conferences and appear in a paper submitted to a special issue of the Journal of Quantum Electronics devoted to tunable lasers. The results of this work will be described in the following.

PAPERS DELIVERED

C. E. Byvik, A.M. Buoncristiani and R. V. Hess. Absorption and Fluorescence of Alexandrite and Titanium in Sapphire and Glass. NASA Workshop on Tunable Solid State Lasers for Remote Sensing, Stanford University, October 1-3, 1984.

A.M. Buoncristiani and C. E. Byvik. Temperature Dependence of the Fluorescence Spectrum of Ti:Al_2O_3. Bull. APS, v29, n9, p1496 (1984).

A.M. Buoncristiani. Quantum Tunneling Through a Dissipative Barrier. Bull. APS, v29, n9, p1500 (1984).

C. E. Byvik, A.M. Buoncristiani and J. C. Barnes. Absorption and Emission Spectra of Titanium in Al_2O_3 and in Transition Metal Titanates. The Electrochemical Society, 167th Meeting Program, p 125c (1984).

C. E. Byvik, A.M. Buoncristiani and J.C. Barnes. Temperature Dependence of the Fluorescence Lineshape and Fluorescence Lifetime of Titanium Doped Sapphire. Technical Digest of the Optical Society of America: Topical Meeting on Tunable Solid-State Lasers, pfTHB2-1 (1984).

C. E. Byvik and A.M. Buoncristiani. Analysis of Vibronic Transitions in Titanium Doped Sapphire using the Temperature Dependence of the Fluorescence Spectra. Submitted to a special issue of the Journal of Quantum Electronics on Tunable Lasers.

II. Review of the Work on Superlattice Structures

A. Background

During the last decade there has been a growing interest in the physical properties of a new type of semiconducting material called a doping modulated superlattice or a NIPI structure, formed by alternating ultrathin layers of n- and p- type materials with the intrinsic semiconductor. [1-3] This growth procedure produces a periodic space charge potential within the material. As a consequence of this periodic potential the local charge carrier concentrations in the crystal can be altered by optical excitation or by charge injection, effectively producing a crystal with variable carrier concentration, variable energy band gap and variable optical absorption characteristics.

These properties appearing in a crystal capable of being grown on a small device scale suggest numerous and diverse electro-optical applications (some of which have already been developed): solid-state lasers, optical sensors and filters, ultrafast switches and a variety of other devices for optical data acquisition and processing. Much of this technological advance, which continues at a rapid pace, bears directly upon the mission of NASA and its need for reliable optical information processing. For example, a device whose optical absorption characteristics can be controlled externally could be used as the basis of a tunable laser detector. Such a device used in concert with a tunable (solid-state) laser could provide a laser communication system able to discriminate a signal from a relatively large background and thus, provide a low power earth-space laser communication system that would operate in daylight.

The techniques for growing NIPI crystals need to be improved before

reliable device structures can be fabricated. For example, the junctions between layers are not as abrupt as they may be and a significant amount of defects and impurities remain as artifacts of the growth technique in NIPI crystals. The purpose of the research described in this proposal was to study how standard electronic and optical measurement techniques can be used to assess the quality of NIPI crystals; then, equipped with this assessment, the crystal growth environment can be monitored to produce crystals of the highest possible quality.

In the early 1970's Esaki and Tsu suggested the possibility of fabricating a superlattice structure by varying the crystalline composition of a semiconductor periodically in one spatial dimension.[1] If the period of this variation were on the order of 50 to 100 A^{O} the individual layers would be large enough to exhibit the collective behavior of a crystalline solid, such as possessing an energy band structure, but small enough, compared, for example to the mean free path of an electron, to distort that band structure from that expected of a uniform crystalline solid. The resulting layered structure would then provide quantum effects on a new superlattice or quantum well scale. Esaki and Tsu suggested two methods for obtaining this periodic variation in structure: one by varying the alloy composition of a semiconductor, the other by varying donor or acceptor levels in a homogeneous semiconductor. The lattice technique has been extensively studied by Döhler[2,3] who has focused attention on structures doped with ultrathin n- and p- layers separated by an intrinsic layer (NIPI structures). The superlattice structures display interesting properties; among the most important are variability of the charge carrier concentrations and variability of the energy band gap. These properties

suggest many useful research and device applications.

Since these early suggestions of the possibilities inherent in semi-conductor superlattice structures there has been a broad based and largely successful research effort to fabricate and to study them.[4] The initial and still dominant superlattice growth technique is molecular beam epitaxy (MBE). Current MBE technology is sufficiently precise to allow the fabrication of the ultrathin superlattice layers having relatively high purity. Recently other growth techniques such as metal organic chemical vapor deposition (MO-CVD) have been used to grow semi-conductor superlattices[5,6] of a quality inferior to, but approaching these grown by MBE. Since it appears that the fabrication of complex devices on an industrial scale would be easier using the MOCVD process there is interest in and a reasonable probability for[7] significantly improving the MO-CVD process. For example, one improvement in the MO-CVD process involves plasma enhancement in which the reactant and carrier gases are mixed and passed into the reaction zone, where a plasma is generated. Plasma enhancement of the reactant gases allows growth to take place on a cooler substrate. The lower temperature of the substrate should result in an improved environment for superlattice growth. Specifically, the lower temperature should reduce the number of thermally generated defects and it should decrease the interdiffusion between adjacent layers, as well as self-diffusion.

B. Work Initiated

The main objective of the research effort proposed here was to be the development of a phenomenological analysis describing how the electronic and optical properties of doping modulated superlattices reflect the environment in which they were grown. Using this description,

the growth environment could be altered to optimize desired properties of the superlattices[8]. The growth environment for plasma enhanced MO-CVD includes the following: temperature of the substrate, characteristics of the feed gas and its flow, and characteristics of the plasma. The general structural characteristics of the superlattice include the doping profile and the distribution of impurities and defects. An array of standard techniques are available to measure the electronic and optical properties of a superlattice: secondary ion mass spectometry determines carrier concentrations, measurement of the Hall effect determines mobilities and photoluminescence experiments determine the overall quality of the crystals.

As described in the synopsis work on this project was terminated for reasons of safety before it could be completed. Nevertheless, several tasks were completed.

(1) An experimental Hall probe was renovated and software for computer control of the experiment was developed. This set-up remains operative and is described in Section III.

(2) Luminescence experiments on solid state laser materials were initiated and results of these experiments appear in Section IV.

(3) Some modeling of electronic transport in superlattices was begun. One part involved integration of the Poisson-Boltzmann equations to develop a semi-classical model of the modulation doped potential. Another part involved use of the method of flux conservation to determine current across the superlattice planes. Neither of these projects was completed before the work on superlattices ended.

III. The Hall Effect Apparatus

The laboratory dedicated to measurements of the electronic and optical properties of III-IV semi-conductor compounds located in Building 1283 at the NASA Langley Research Center had a Hall probe apparatus which was inoperative. Part of the work on this grant was expended in renewing the apparatus and in developing a computer code to control the experiment. The technique of the measurement follows a method developed by van der Pauw[9-11] and are described in the ASTM Standards document F76[12].

The basic idea of the measurement procedure is as follows; Consider a single crystal lamelar sample with four contacts, refer to Figure 1. To measure the resistivity of the sample pass a measured current I through two adjacent contacts, say 1 and 2, and measure the voltage V across the other contacts. Form the quantity $R = |V/I|$. Now pass a measured current I^1 through the next pair of contacts, say 2 and 3, and measure the voltage V^1 across the other contacts. Form the quantity $R^1 = |V^1/I^1|$. Now, as was shown by van der Pauw [9], the resistivity ρ of the sample with thickness t is related to R and R^1 through the transcendental relation;

$$\exp(-\pi\ tR/\rho) + \exp(-\pi\ \ t\ \ R^1/\rho) = 1$$

To measure the Hall coefficient pass a measured current I through two non-adjacent contacts of the sample, say 1 and 3, and measure the voltage V across the other two contacts and form $R = |V/I|$. Now turn on a magnetic field B perpendicular to the sample repeating the measurements to obtain $R^1 = |V^1/I^1|$. The Hall coefficient R_H is then given by the relation

$$R_H = \frac{t}{B}\ |R^1 - R|$$

and the Hall mobility μ by

$$\mu = R_H / \rho$$

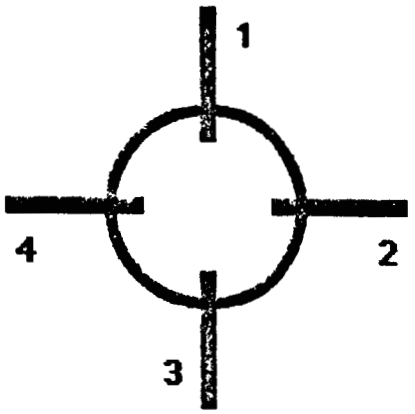

[a] Schematic Diagram of the Sample

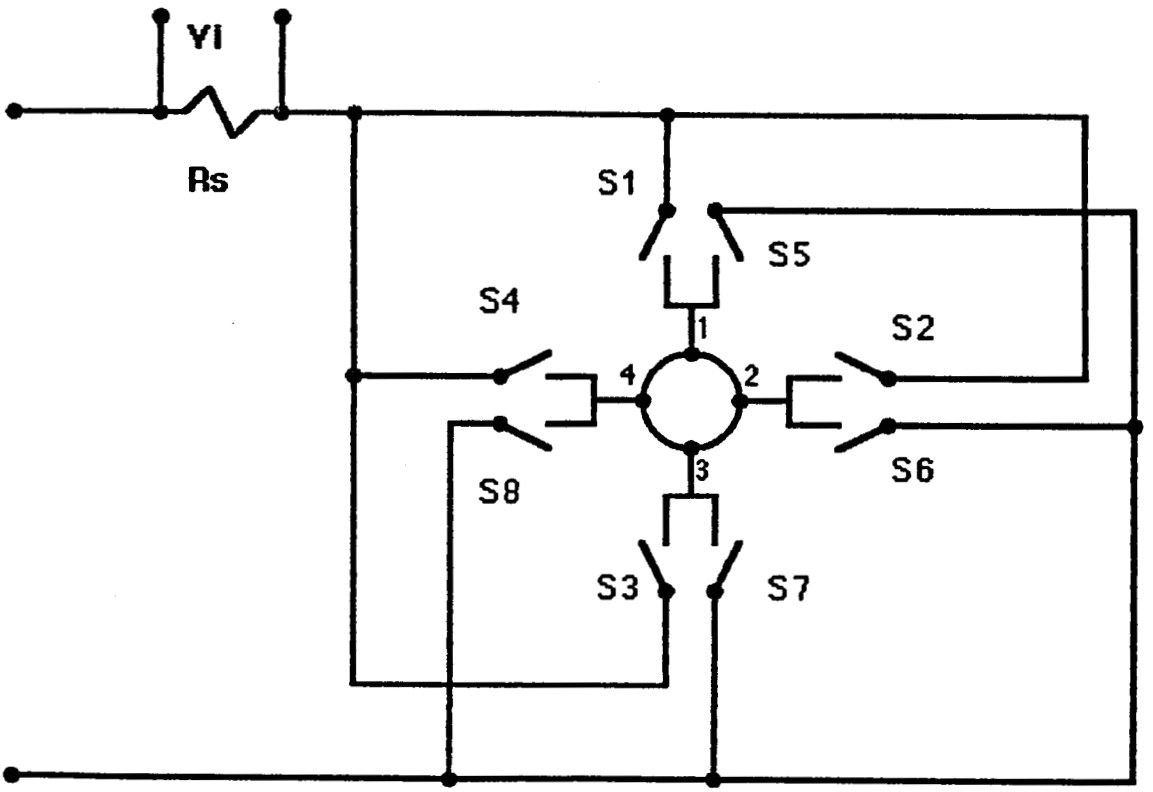

[b] Schematic Diagram for Current Steering

Figure 1

FLOW CHART FOR MEASUREMENT PROGRAM

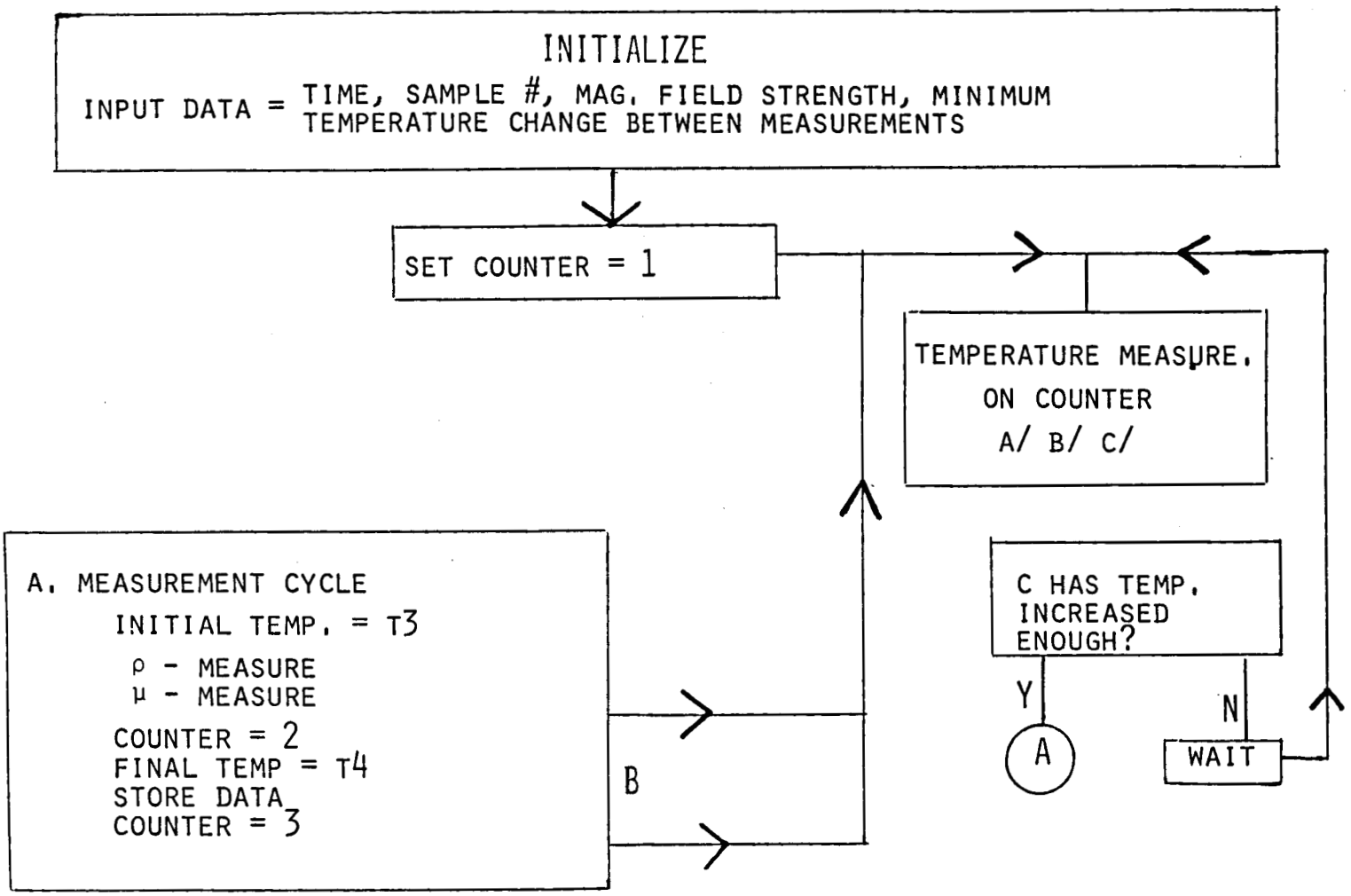

TABLE 1

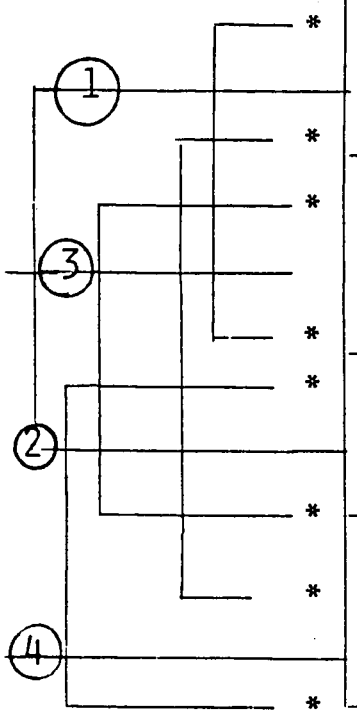

1 2 3 4 5 6 7 8 6 8 10 12 7 9 11 13	CURRENT I_{XY}	$V_B - V_A$ + -	S_0 S_1 S_{11} S_2 S_{12} S_{13} 0 1 2 3 4 5
C C C	1 2	3 4	C C
C C	1 3	2 4	C C
C C	1 4	2 3	C C
C C	2 3	1 4	C C
C C	2 4	1 3	C C
C C	2 1	3 4	C C
C C	3 4	1 2	C C
C C C	3 1	2 4	C C
C C	3 2	1 4	C C
C C C	4 1	2 3	C C
C C	4 2	1 3	C C
C C	4 3	1 2	C C

SWITCH SETTINGS FOR HALL MEASUREMENTS

TABLE 2

DATA STORED FROM MEASUREMENT PROGRAM

Y(N,C)	$1 \leq N \leq 34$	Data Points from 1 run
	C = 1, 2 ...	60 Identifies a Run

N-data points	Y(N,C)
B = 0	1. V32
	2. V(Rs)12
	3. V23
	4. V(Rs)14
	5. V14
	6. V(Rs)23
	7. V34
	8. V(Rs)21
	9. V12
	10. V(Rs)34
	11. V14
	12. V(Rs)32
	13. V23
	14. V(Rs)41
	15. V12
	16. V(Rs)43
B > 0	17. V24
	18. V(Rs)13
	19. V24
	20. V(Rs)31
	21. V13
	22. V(Rs)24
	23. V43
	24. V(Rs)42
B < 0	25. V24
	26. V(Rs)13
	27. V24
	28. V(Rs)31
	29. V13
	30. V(Rs)24
	31. V13
	32. V(Rs)24
	33. T Start
	34. T Finish

Data Stored as $|V|*1000$

Data Transferred as COMMON: Mag, Sample, TO

Table 2'

blue shifted by about 150nm. We undertook a study of Ri(III) in glass hosts which should exhibit an extreme low field case for the ion[14].

The degeneracy of 3 d electron energy levels in free transition metal ions is broken by the Jahn-Teller effect when these ions are substitutionally-doped into a crystal host. The magnitude of this splitting depends primarily on the crystal field at the substituted ion and as a result the coupling between the electronic states and the host lattice is strong. Phonon coupled electronic transitions between the split levels provide the broad emission spectrum required for tunable solid state lasers. The theoretical foundations for phonon terminated electronic transitions (vibronic transitions) were published 20 years ago by McCumber[15-16] and ten years passed before it was discovered that alexandrite (13), chromium doped chrysoberyl, provided a medium for tunable lasing in the optical region. Since then the chromium ion has been doped into emerald[17,18] and gadolinium scandium gallium garnet (GSGG)[19] and shown to provide tunable solid state lasing media. The ions Co^{2+}, N_2^{2+} and V^{2+} have been shown to provide tunable laser action in the IR in solid hosts[20].

Recently, Moulton reported[21,22] tunable lasing in the optical region with titanium doped sapphire. This new material offers some advantages over chromium doped hosts. The Ti^{3+} ion in a crystalline environment such as sapphire exhibits a large stokes shift and a broader tuning range than Cr^{3+}. In addition, excited state absorption, which inhibits operation of the alexandrite laser at temperatures above 200K, is negligible since in $Ti:^{3+}:Al_2O_3$ the higher energy states are too high to be a significant loss mechanism. Also, the stimulated emission cross section of Ti^{3+} in sapphire is about an order of magnitude higher than in alexandrite.

Because of these advantages, it is important to delineate and characterize

the properties of Ti^{3+} in various crystalline hosts that may be important to the performance of tunable solid state lasers. This information is useful not only for improving existing laser materials but also for an effective search for new tunable solid state materials. Since the existence of vibronic transitions is necessary for a solid state laser to be tunable and since Ti^{3+} doped into sapphire is one of the promising candidates for a tunable solid state laser system, our research program includes experiments which examine the phonon processes giving rise to the broad band fluorescence observed for this material. We report here the results of an experimental investigation of the temperature dependence of the fluorescence spectrum of Ti^{3+} doped sapphire.

EXPERIMENTAL

Czochralski grown samples of sapphire rods doped with Ti^{3+} to a suppliers[2,3] stated level of 0.09% were cut and polished into wafers approximately 1cm in diameter and 2mm thick. The crystal c-axis was oriented 60^{o} with respect to the normal to the surface of the wafer. The wafer was placed in a resistance heated aluminum block for the high temperature data and on a copper heat sink attached to a helium refrigerator for the low temperature data. The temperature of the sample was controlled to within 1K during the recording of the emission spectrum. Fluorescence was stimulated by the 514.5nm line of an argon ion laser. The continuum radiation from the laser was filtered with a laser line filter having a transmission bandwidth of less than 3nm at 514.5nm. The beam was focused on the wafer. A color filter passing radiation longer than 540nm was placed at the entrance slit of the monochromator to filter the scattered laser radiation. The stimulated emission from the sample was focused onto the entrance slit of a 1.25 meter monochromator and detected by a thermoelectrically cooled GaAs photomultiplier

tube. The laser power was monitored by directing a portion of the laser beam onto a thermopile detector. The incident laser power varied less than 3% during the recording of the emission spectrum.

RESULTS AND DISCUSSION

Theoretical and experimental studies of the optical and infrared spectra of Ti^{3+} in Al_2O_3 have been reported[24-29]. The results of this early work indicated the Ti^{3+} ion substitutes for the Al^{3+} and is surrounded by 6 oxygen ions resulting in octahedral ligand symmetry as shown in Figure 2(a). The symmetry of the single 3 d electron is broken by the Jahn-Teller effect[25,26] through a distortion of the octahedron. The energy level diagram for the $3d^1$ ion perturbed by a large cubic field component, smaller trigonal field and spin-orbit couplings is shown in Figure 2(b). In addition, the ^2Eg and ^2T2g states are effected by the dynamic Jahn-Teller interaction. A simplified schematic diagram of the adiabatic potential curves for these two states are shown in Figure 2(c).

The fluorescence spectra at various temperatures from 13K to 578K shown in Figure 3 are due to vibronic transitions between the two Jahn-Teller distorted electronic states ^2Eg and ^2T2g. The room temperature spectrum is structureless except for an emission doublet near 690nm. This doublet is attributed by Gachter and Koningstein[29] to chromium unintentionally doped into the host. The rapid drop in emission intensity above 870nm is due to the spectral response of the photomultiplier used in these experiments. The fluorescence intensity was found to decrease as the sample temperature increased. In particular, the spectrum at 578K is 50 times less intense than the room temperature spectrum. Line broadening and a red shifting of the peak of the emission spectra accompanies an increase in sample temperature.

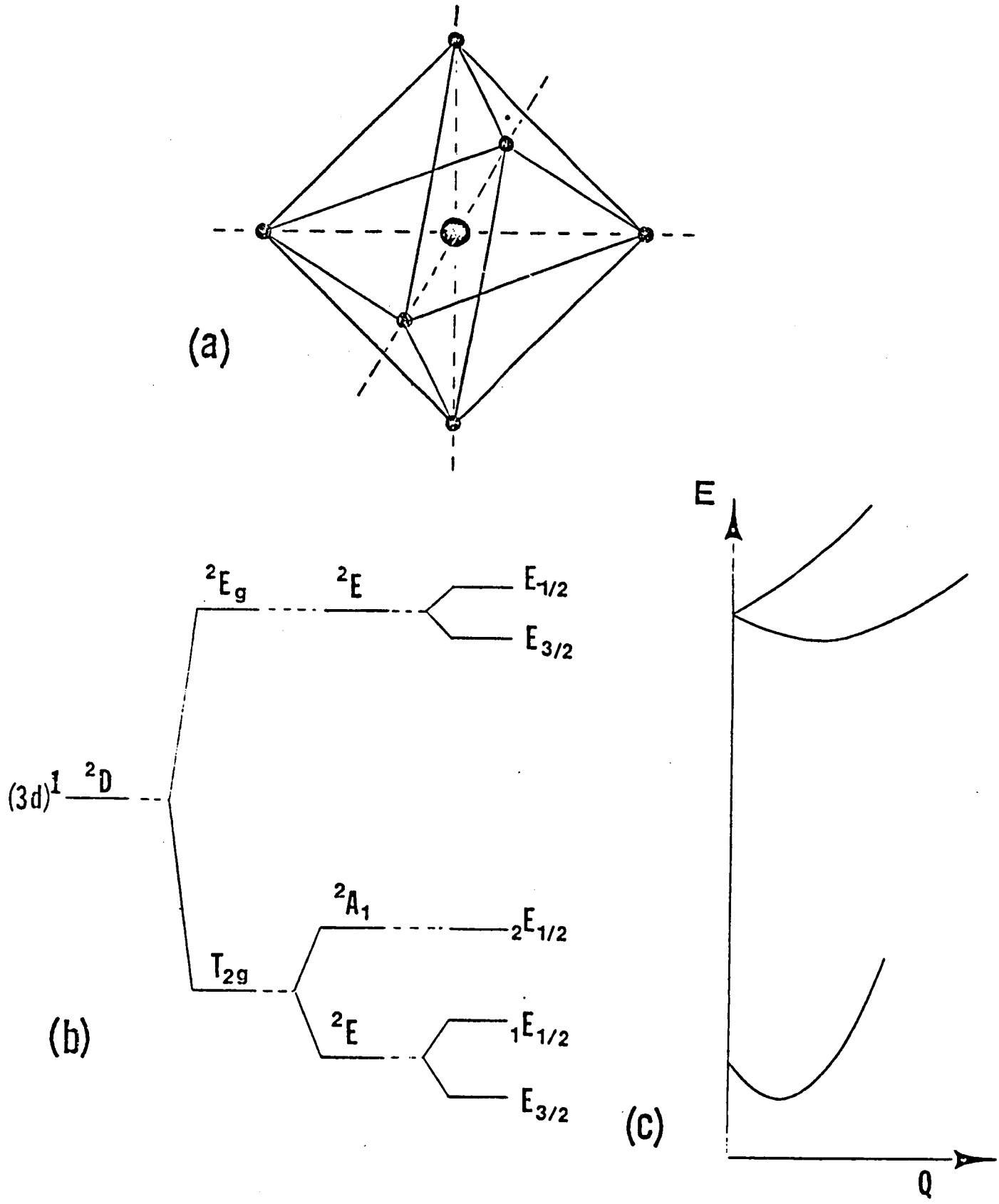

FIGURE 2.

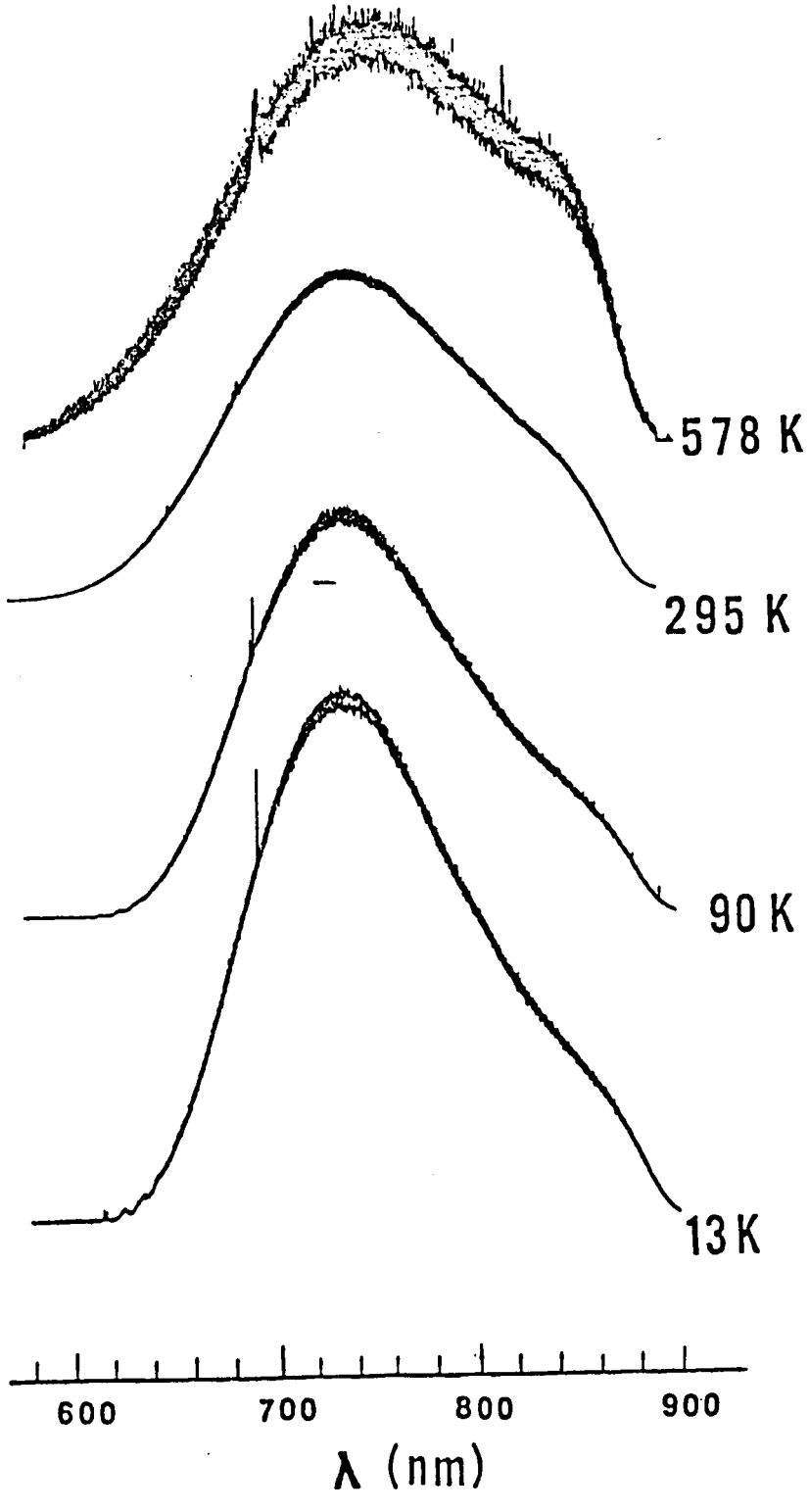

FIGURE 3.

Additional structure can be seen at low temperatures on the high energy side of the emission spectra. These lines are due to th- zero-, one-, two-, etc., phonon assisted electronic transitions. These electronic and vibronic transitions can be more easily seen in Figure 4 which displays the high energy region on a more sensitive scale. At 13K three zero-phonon transitions can be identified. Two strong, narrow peaks are apparent at 616.5nm (16,220.6cm $^{-1}$) and 617.97nm (16,181.9cm^{-1}) and correspond to transitions from the lowest vibrational state of the ^{2}Eg level to the ground states $E_{3/2}$ and $_{1}E_{1/2}$, respectively. A third, broad, weak zero-phonon transition peaking at 620.6nm (16,113.4cm^{-1}) corresponds to a transition to the $_{2}E_{1/2}$ state. The energy difference between $_{1}E_{1/2}$ and $E_{3/2}$ defined as δ_1 = 38.7cm^{-1} and that between $_{2}E_{1/2}$ and $E_{3/2}$ defined as δ_2 - 107.2cm^{-1} are given in Table 3. Our values for δ_1 and δ_2 agree with those of Gachter and Koningstein[29] obtained from fluorescence spectra of Verneuil grown material as well as with values obtained from infrared spectra[27,28] and those predicted from theoretical considerations[25,26]. The line widths of the two high energy zero-phonon lines, $\Delta\nu_1$ and $\Delta\nu_2$, are 11.5cm^{-1} and 13.1cm^{-1} at 13K. These line widths are broader than reported by Gachter and Koningstein (29) (See Table 3). This difference is attributed to variation of the inhomogeniety of the host crystals from sample to sample. Post growth treatments of the Czochralski grown samples may reduce the line width of these zero-phonon lines.

Superimposed upon the rising emission spectrum on the low energy side of the zero phonon lines are three structures which can be identified as one-, two-, and three-phonon assisted transitions. The first group of three lines are consistent with single phonon transitions from the zero point level of the upper ^{2}Eg state to the first phonon state the ^{2}Tg levels.

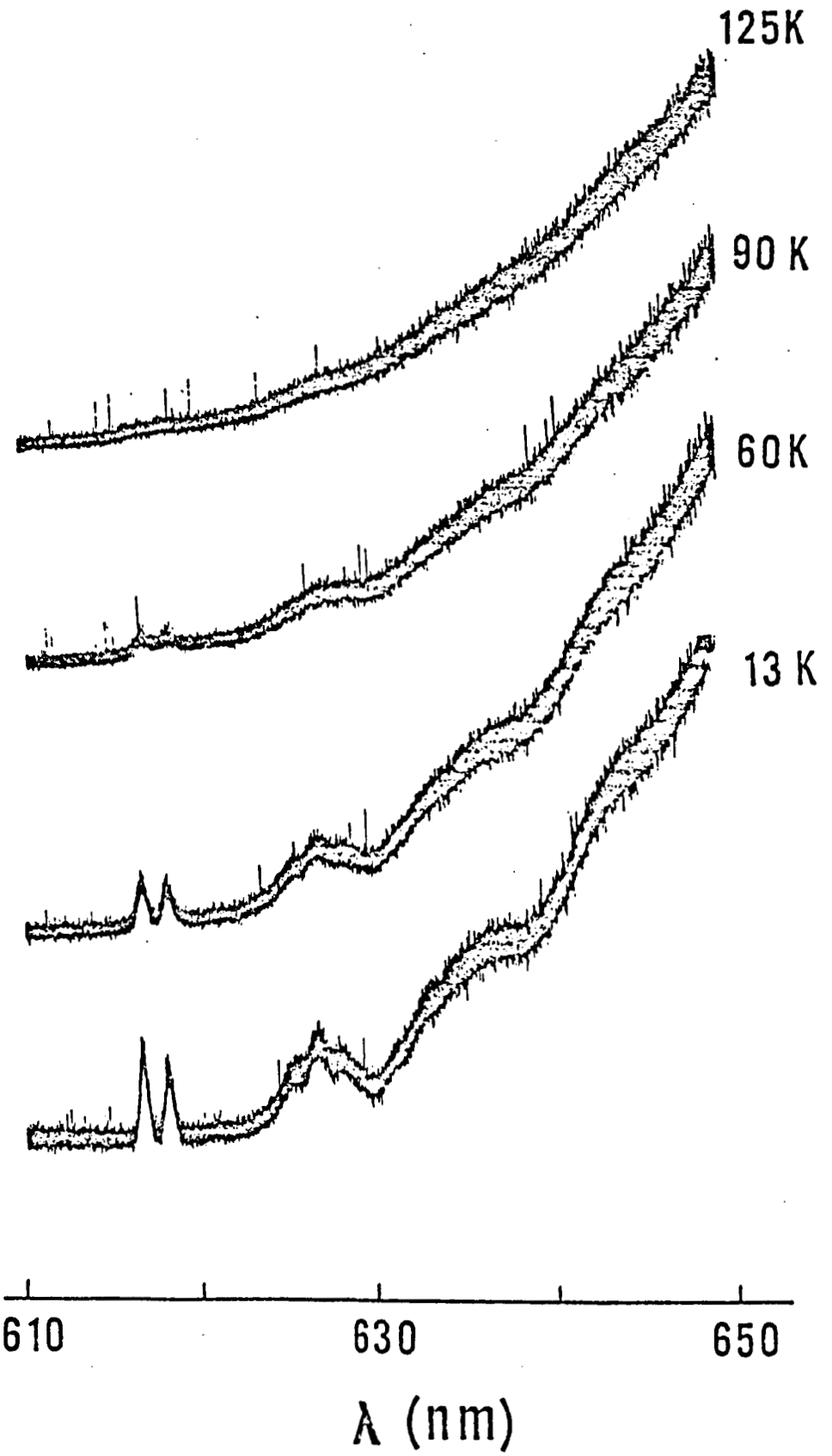

FIGURE 4.

Evidently, two distinct phonon energies are associated with the ^2Tg levels indicating that two modes of lattice vibration couple to the electronic energies. These phonon energies, labeled $h\nu_{g1}$, and $h\nu_{g2}$ in Table 3, were measured in this experiment to be $222cm^{-1}$ and $260cm^{-1}$. The second and third groups of lines are due to two-and three-phonon transitions. This structure disappears at temperatures above 125K. At 80K, fluorescence is observed at $173cm^{-1}$ ($h\nu_e$ in Table 3) on the high energy side of the zero-phonon lines. (Not apparent from Figure 3). This is due to transitions from the first phonon state of the ^2E_g to the zero-point level of the ground ^2T_g term. These values for phonon energies are close to those reported in the literature (37) for Verneuil grown samples. (See Table 3).

Table 3 also includes the position of the absorption peak, Δ, observed in this work and reported by others. The value of 10Dq is given for comparison. In addition, the emission peak ν_F observed by us is significantly different from the value reported in Ref. 29 . This discrepancy may be due to the response of the detector used by Gachter and Koningstein and not due to the difference in the method of growing the samples. The values of the Jahn-Teller energies for the T_{2g} state (E^gJT) and the ^2E_g state (E^eJT) are also included.

The width of the fluorescence spectrum increases with increasing temperature as evident in Figure 3 and the details of this increase are displayed in Figure 5. Measured values of the full width at half-maximum for temperatures ranging from 13K to 578K are represented by circles. The solid curve is a least square fit of these data to the formula

$$\Delta\nu(T) = \Delta\nu(o) \tanh [(n\omega/2kT)]^{-1/2} ,$$

which represents the broadening of an electronic line from its width at T=0, $\Delta\nu(o)$, by means of a single harmonic interaction with phonon energy

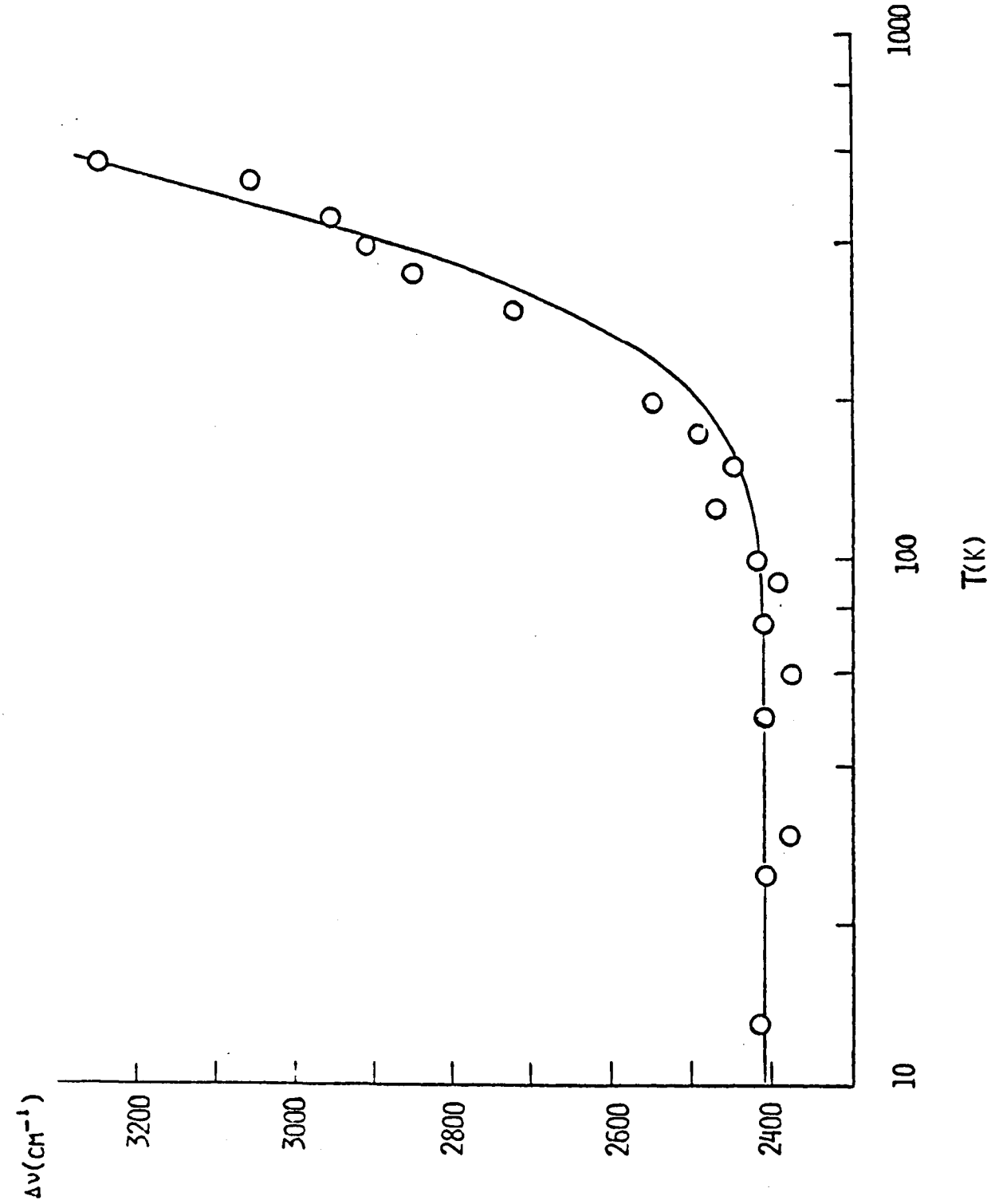

FIGURE 5.

$n\omega$. The least square fit occurs for the values $\Delta\nu(o) - 2420.2cm^{-1}$ and $n\omega = 492cm^{-1}$. As mentioned previously, the low temperature spectrum for the zero and one phonon transitions indicates two active harmonic interactions with phonon energies of 222 and $260cm^{-1}$, respectively, while the high temperature behavior has been fit to a single mode model with characteristic phonon energy approximately equal to the sum of the two low temperature modes. Some idea of the mechanism of this increase in width can be given by examining how the high and low energy half maximum points separately changes with temperature. Curves showing how two frequencies associated with the half maximum, νmax and νmin, change with temperature are displayed on Figure 6.

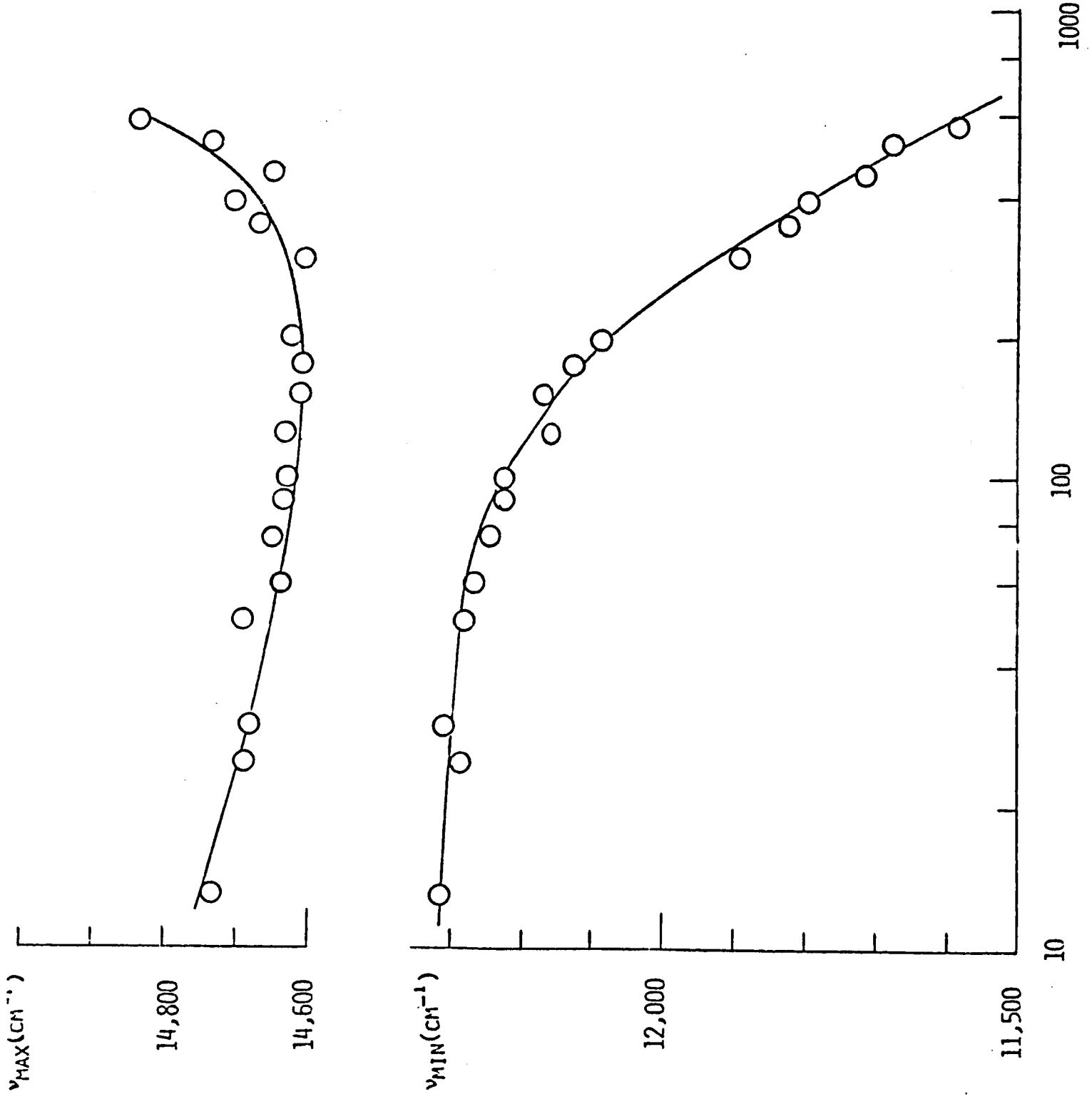

FIGURE 6.

Bibliography

1. L. Esaki and R. Tsu, IBM J. Res. Develop. 14, 61 (1970).

2. G.H. Döhler, Phys. Stat. Sol (b) 52, 79 (1972).

3. G.H. Döhler, Phys. Stat. Sol (b) 52, 533 (1972).

4. L.L. Chang, J. Vac. Sci. Technol B 1(2), 120 (1983).

5. P.M. Frijlink and J. Maluenda, Japanese J. of Appl. Phys. 21 (9), 1574 (1982).

6. M. Erman and P.M. Frijlink, Appl. Phys. Lett. 43(3), 285 (1983).

7. J.E. Andrews, Res. and Dev. 26, (2) 183 (1984).

8. K. Ploog and G.H. Döhler, Adv. in Phys. 32 (3) 285 (1983).

9. J. J. van der Pauw, Phillips Research Reports vol 13, no. 1, 1 (1958).

10. A. C. Baer, Solid-State Electronics, vol 9, 339 (1966).

11. R. Chwang, B. J. Smith and C. R. Crowell, Solid-State Electronics, vol 17, 1217 (1974).

12. _____, Measuring Hall Mobility in Extrinsic Semiconductor Single Crystals, ASTM Standards Designation F76-67T.

13. J. C. Walling, O. G. Peterson, H. P. Henssen, R. C. Morris, and E. W. O'Dell, IEEE J. Quantum Electr., vol QE16, 1302 (1980).

14. P. T. Kenyon, L. Andrews, B. McCollum and A. Lempici, IEEE J. Quantum Electr., vol QE18, 1189 (1982).

15. D. E. McCumber, Theory of phonon-terminated optical laser. Phys. Rev., vol 134, ppA299-A306, 1964.

16. D. E. McCumber, Einstein relations connecting broadband emission and absorption spectra. Phys. Rev., vol 136, ppA954-A957, 1964.

17. J. Buchert, A. Katz and R. R. Alfano, Laser action in emerald. IEEE J. Quantum Electr., vol QE19, pp1477-1478, 1983.

18. M. L. Shand and J. C. Walling, A tunable emerald laser. IEEE J. Quantum Electr., vol QE18, pp1829-1830, 1982.

19. E. V. Zharikov, N.N. Il'ichev, S. P. Kalitin, V.V. Laptev, A.A. Malyutin, V.V. Osiko, V.G. Ostroumov, P.P. Pashinin, A.M. Prokhorov, V.A. Smirnov, A.F. Umyskov, and I.A. Shcherbakov, Tunable laser utilizing an electronic vibrational transition in chromium in a gadolinium scandium gallium garnet crystal. Sov. J. Quantum Electr., vol 13, pp1274-1276, 1983.

20. L. F. Johnson, H. J. Guggenheim and R. A. Thomas, Phonon-terminated optical masers. Phys. Rev., vol 149, pp179-185, 1966.

21. P. F. Moulton, Recent advances in solid state lasers. Conference on Lasers and Electro-Optics, June 19-22, 1984, Anaheim, CA, Paper WA2.

22. P. F. Moulton, Tunable paramagnetic ion lasers. Laser Handbook Vol. 4, Michail Bass and Malcolm Stitch, eds. (North Holland, Amsterdam, in press).

23. The Ti: Sapphire samples were supplied by the Electronics Division of Union Carbide Corporation, San Diego, CA.

24. D. S. McClure, Optical spectra of transition-metal ions in corundum. J. Chem. Phys., vol 36, pp2757-2779, 1962.

25. R. M. McFarlane, J. T. Wong and M. D. Sturge, Dynamic Jahn-Teller effect in octohedrally coordinated d^1 impurity systems. Phys. Rev., vol 166, pp250-258, 1968.

26. L. Cianchi, M. Mancini and P. Moretti, Influence of covalency in the dynamic Jahn-Teller effect in $Al_2O_3:Ti^{3+}$. Phys. Rev., B, vol 7, pp5014-5017, 1973.

27. E. D. Nelson, J. Y. Wong and A. L. Schawlow, Far infrared spectra of $Al_2O_3:Cr^{3+}$ and $Al_2O_3:Ti^{3+}$. Phys. Rev., vol 156, pp298-308, 1967.

28. R. R. Joyce and P. L. Richards, Far-infrared spectra of Al_2O_3 doped with Ti, V, and Cr. Phys, Rev., vol 179, pp375-380, 1969.

29. B. F. Gachter and J. A. Koningstein, Zero phonon transitions and interacting Jahn-Teller phonon energies from fluorescence spectrum of α-$Al_2O_3:Ti^{3+}$. J. Chem. Phys., vol 60, pp2003-2006, 1974.

Figure Captions

Figure 2. (a) The ideal octahedral site of the titanium ion (large circle surrounded by six oxygen ions (small circles) in sapphire. (b) Term splitting of $(3d)^1$ state. Starting from the left; the free ion, splitting by a cubic field, effect of a trigonal field, then spin-orbit coupling. (c) Simplified schematic diagram of the adiabatic potential curves for the $^2T_{2g}$ and the ^2E_g states of Ti^{3+} in sapphire.

Figure 3. The uncorrected fluorescence spectra of Ti^{3+} in sapphire as a function of sample temperature. The sharp drop on the right side of the spectra is due to the response of the GaAs Photomultiplier tube. The 578K spectrum has been simplified 50 times that of the 295K spectrum.

Figure 4. The temperature dependent fluorescence spectra showing the zero, single, and higher phonon assisted electronic transitions.

Figure 5. Temperature dependence of the full-width points, ν_{max} and ν_{min} at half maximum of the fluorescence spectra. The difference, $\nu_{max} - \nu_{min}$ at any temperature is the linewidth. See Figure 5..

Figure 6. Temperature dependence of the linewidth at half maximum of the fluorescence spectra.